Conference Paper, Published Version

Mooyaart, Leslie; Peters, Dirk Jan; Kerpen, Nils; Huis in 't Veld, Menno

Design Aspects of Torqued Concrete Column Revetments

Coastal Structures 2019 - Nils Goseberg, Torsten Schlurmann (eds) - © 2019 Bundesanstalt für Wasserbau
ISBN 978-3-939230-64-9 (Online) - DOI: 10.18451/978-3-939230-64-9_034

Design Aspects of Torqued Concrete Column Revetments

L. F. Mooyaart
Royal HaskoningDHV, Amersfoort, The Netherlands

D. J. Peters [1,2]
[1]Royal HaskoningDHV, Rotterdam, The Netherlands
[2]Delft University of Technology, Delft, Netherlands

N. B. Kerpen
Leibniz University Hannover, Ludwig-Franzius-Institut for Hydraulic, Estuarine and Coastal Engineering, Hannover, Germany.

M. Huis in't Veld
Boskalis, Papendrecht, The Netherlands

Abstract: Coastal defences are protected by revetments to prevent erosion of the embankment. Many different types of revetments exist. Pattern-placed concrete columns are favourable because they are relatively light compared to the hydraulic load. However, at transitions below the design water table, normal pattern-placed concrete columns are weak. Torqued concrete columns are interlocking and can increase the strength of the revetment at this transition. This paper describes the design aspects of torqued concrete columns and the large-scale flume testing of this revetment type.

Keywords: Coastal defence, design, revetments, concrete columns, large-scale flume test

1 Introduction

Single pattern-placed revetments clad dikes bordering relatively shallow waters in tidal areas. A typical cross section consists of a foreshore with a sloping seabed of m = 0.01 to 0.03, a toe structure and a dike with a protected slope of 1:3 to 1:5. Toe structures extend below mean sea level, which are constructed around low tide. Due to the foreshore, wind waves are depth-limited during storm conditions, and the most severe conditions on Dutch coasts are in the order of H_{m0} = 2 to 3 m.

Protecting the slope with pattern-placed revetments creates a smooth surface, avoiding direct wave and current forces on the revetment elements. Uplift forces are hence the most severe design load. At pattern-placed revetments, the magnitude of the pressure build-up is determined by the permeability of the top layer and the thickness and permeability of the first underlayer. The regular placing of the revetment contributes to the coherence of the structure. This coherence leads to more resistance than the self-weight of the individual elements only (Bolderman & Dwars, 1919, Huitema, 1947). Peters (2017) found the amount of coherence to be related to the weight of the concrete columns above the lifted part of the revetment. Subsequently, thin revetments tend to become unstable when the slope is insufficiently extended towards the higher part of the dike, i.e. when the top of the revetment surface is too close to the water table (for damage reports refer to Klein Breteler, 1992).

Berms or outside shoulders are often part of the dike design to limit wave run-up and overtopping, reducing crest height, to provide stability against geotechnical failure mechanisms, to reduce settlement risks, and to offer vehicle and pedestrian access at the outside slope, for maintenance and recreational purposes. For the Afsluitdijk revision tender, a berm below design water level was required and a pattern-placed revetment was designed for the lower slope, which is fully submerged during storm surge conditions. To improve the stability performance for the severe design wave condition (H_{m0} = 4.2m), a pattern-placed revetment with physical interlocking was preferred. The

design was carried out by a team of RHDHV, led by Boskalis and Volker Wessels, operating under the name Corneel.

This article aims at finding an economic solution for the set-back in stability of pattern-placed revetments just below the top of a continuous revetment slab. A solution is found in applying wedged interlocking elements (see Fig. 1). This shape variation mobilizes axial movement before the element can be lifted, resulting in additional resistance against uplift. The wedge shapes form a physical interlock, but the working principle of this concrete column is modelled as a direct increase of frictional interlocking. Since the location of the wave impact varies during storm conditions, the wedge shape must potentially work in two directions. Therefore, the elements are designed as having alternating orientations of the element-to-element interface. Furthermore, pattern-placed revetments need to be geometrically flexible. Therefore, the system needs to be articulated and as such able to adjust itself to settlement and formation of cavities and erosion of the underlayers. Any form of physical interlocking of elements shall not compromise the articulative feature of the system.

.

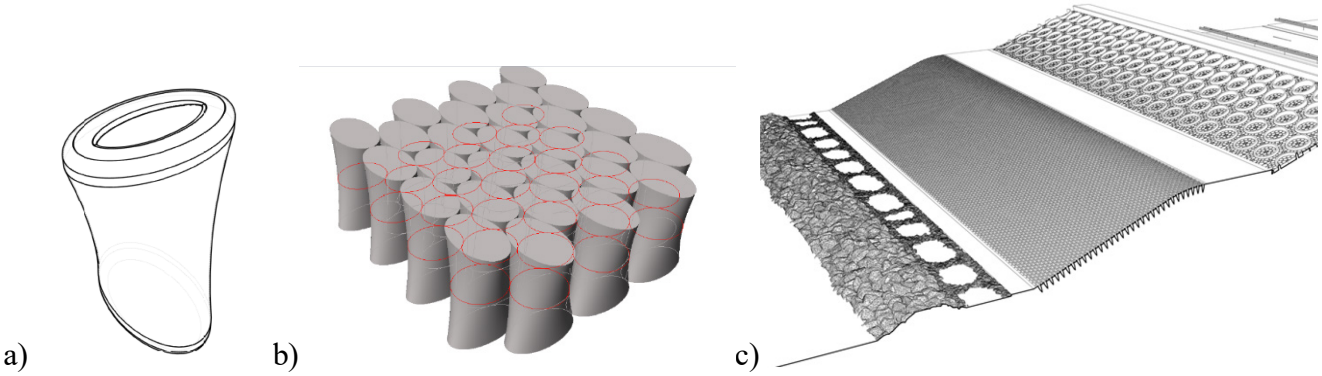

Fig. 1. Two-sided wedge interlocking element (left) and tender design Afsluitdijk with torqued concrete columns in lower slope (right)

2 Model description

The resistance of a pattern placed revetment to withstand destabilizing uplift loads relies on the self-weight and on frictional interlocking. A basic beam model is applied to describe the physics of the frictional interlocking (see Fig. 2). The beam model represents a strip of pattern placed prismatic concrete elements which have joints perpendicular to the beam axis. As the revetment strip finds itself on a slope, gravity forces lead to axial forces (q_x) and to holding down forces ($q_{z'}$). The beam is assumed to have zero friction at the interface with the underlayer and, subsequently, the beam needs support by the toe structure. Wolters (2007) found this assumption to be realistic and this paper also confirms the reality of this assumption.

If individual revetment elements are loaded with uplift forces beyond their self-weight component $G_{z'} = (\rho_s - \rho)\, gDB \cos\alpha$, equilibrium can still be found. Gravity causes a normal force in the beam, which enables the beam to resist shear forces. If the pulled element has a location z_{pull}, which is $z_{top} - z_{pull}$ below the top of the revetment, the normal force at that location is:

$$N_2 = \int q_x dx = (z_{top} - z_{pull})(\rho_s - \rho)gD, \text{ with } q_x = (\rho_s - \rho)gD \sin\alpha \quad (1)$$

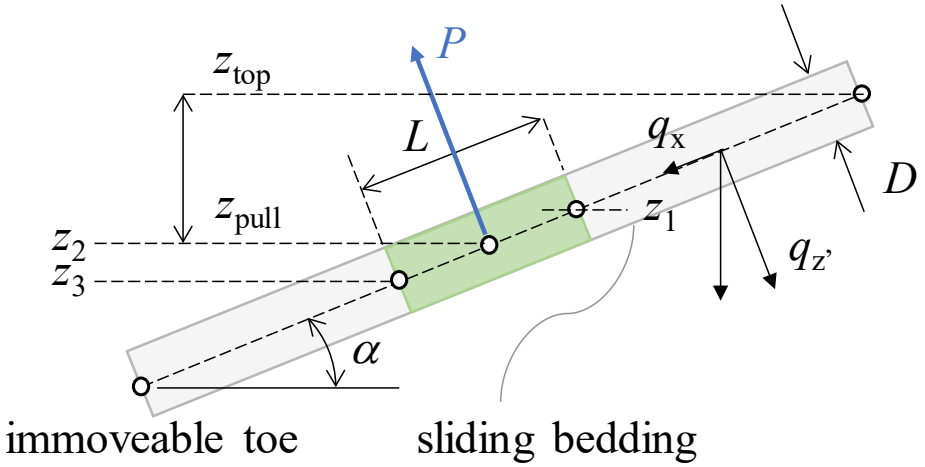

Fig. 2. Beam model with confined section that equals the generalized uplift force.

The capacity for shear force is $V_R = \mu N_2$ per joint. Subsequently, the capacity to resist P equals $G_{z'} + 2 V_u$. If the pull force increases beyond the weight of three elements, or if more elements are loaded at the same time, the rotational equilibrium needs to be considered as well (see Fig. 3). Solving the rotational equilibrium demonstrates the magnitude of additional resistance through frictional interlocking. Therefore, the equilibrium equations of an isolated, confined portion of the beam are derived. The beam weight is, conservatively, assumed to equal the submerged weight over the full length. The portion of the beam that experiences uplift load is assumed to be subject to a single point load, resulting in ease and transparency of the equations.

The uplifted beam portion has a length L, which is defined as the length between zero-shear points, and hence $L = P / q_{z'}$. The joints in the beam have rotational flexibility and, subsequently, bending moments caused by P and $q_{z'}$ are redistributed like in plastic beam. Averaged bending moments will then be sufficient to justify the equilibrium. The maximum bending moment caused by the loads is $M_E = {}^1/_{16}$ P L. The maximum shear force is $V_E = ½$ P. In the failure mode, the maximum bending moment occurs at three locations: as a negative peak at the location of the pull force (point 2), and as positive maxima at both ends of the confined beam (point 1 and 3). The maximum shear force occurs at both sides of the pulled element. In the beam equations the influence of the width B of the individual element is neglected. The capacity for M is given as $M_{Ri} = N_i$ e, with e = 0.4 D. The capacity for V is $V_{Ri} = \mu N_i$.

$$N_i = \int_{x_i}^{x_{top}} q_x dx, \text{ with } q_x = (\rho_s - \rho) g D \sin\alpha \qquad (2)$$

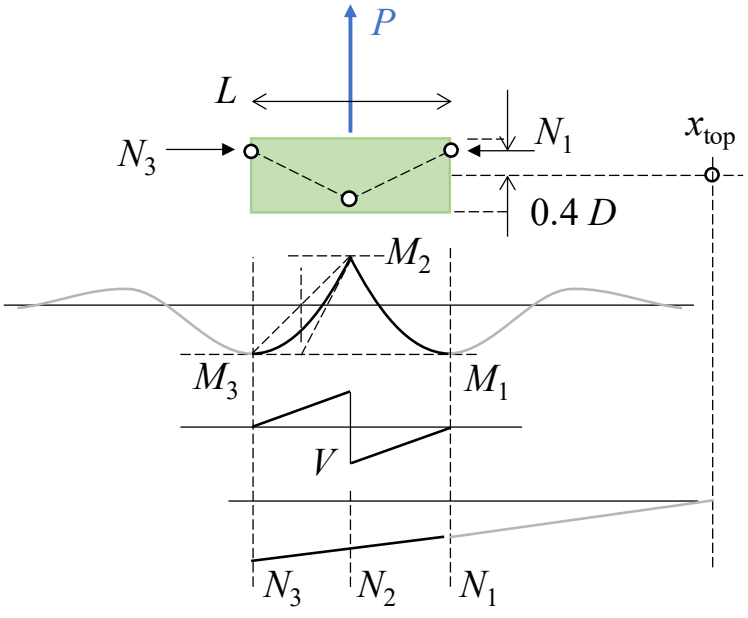

Fig. 3. Equilibrium model of confined section and bending moment and shear force diagrams.

The capacity for P follows from the equilibrium $\sum M_{Ei} = \sum M_{Ri}$ after checking if $V_E < V_R$. The summation (or averaging) of the bending moments shall be done following: $\sum M = {}^1/_4 (M_1 + 2M_2 + M_3)$. To find the solution, iterative computing is required. When M_E is smaller than M_R, the length L can be increased, which is associated with a larger value of P. When L increases, z_1 is kept below z_{top} and z_3 is kept above z_0, the lower end of the revetment beam. Following this procedure for a variable $z_{pull,}$ it is found that P decreases when the pulled element is closer to the top. Consequently, high attacked points have a low resistance, relatively.

At a wave attacked slope, the highest concentration of uplift forces is normally between 0.5 and 1.5 wave height below the still water line, depending on the breaker parameter (i.e. Iribarren number). Plunging waves occur with a Iribarren number around 1 to 1.5 cause peak wave pressures around 0.5 H below the water line.

Wedge-interlocking revetment elements cannot displace upward without moving the neighbouring blocks sideward (see fig. 4). Since the toe is considered immovable, the elements can only move upward. The interface between top and underlayer is a normal concrete-to-gravel interface. Sliding of elements will generate friction (Schoen, 2003, Peters, 2017). Moderate to strong wave action causes cyclic uplift and resets the friction force on the interface between top and underlayer to zero. The complete revetment beam is progressively resting against the toe without experiencing friction. Still, severe wave attack will cause uplift and associated upward sliding of the upper portion of the revetment beam, which generates friction forces. Hence, this friction action is added in the model for a wedge-interlocked revetment system. Therefore, a friction term is added to the sliding model for normal elements:

$$N_1 = \int_{x_1}^{x_{top}} (q_x + \mu q_{z'}) dx, \text{ with } q_x = (\rho_s - \rho) g D \sin\alpha \text{ and } q_{z'} = (\rho_s - \rho) g D \cos\alpha \text{ and } \mu = 0.6$$

$$N_2 = N_1 + \int_{x_2}^{x_1} q_x dx, \text{ and}$$

$$N_3 = N_2 + \int_{x_3}^{x_2} q_x dx \qquad (3)$$

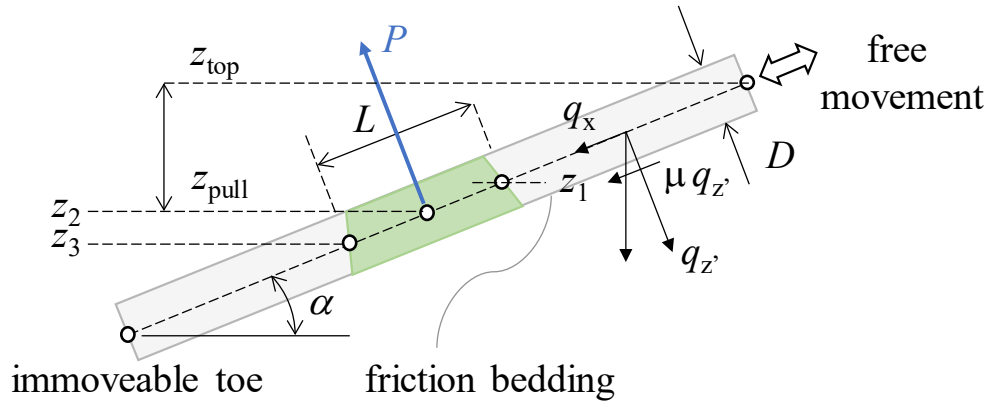

Fig. 4. Model definition with wedge-interlocked section and friction bedding.

Applying these formulas for a case with a 1:3 slope, the system is found to be significantly more stable (i.e. >15%) for values of $(z_{top} - z_2)/D$ of 2. Consequently, a straight slope up to the top with wedge-interlocked elements does not perform better at the top $(z_{top} - z_2)/D < 2$. To improve the stability, the slope is extended with a curved transition section (see Fig. 5). This transition avoids a sharp angle between the slope and the berm. Another benefit of the curved transition is the influence on the wave breaking process. As the slope widens, the waves tend to break further away from the top of the revetment. With a curved upper section, wave impacts hitting the top of the revetment become unlikely. The suggested radius is R = 10 to 30 D. In the curved section, the compressive normal force itself creates uplift. So, a too small radius will create a dominant destabilizing force.

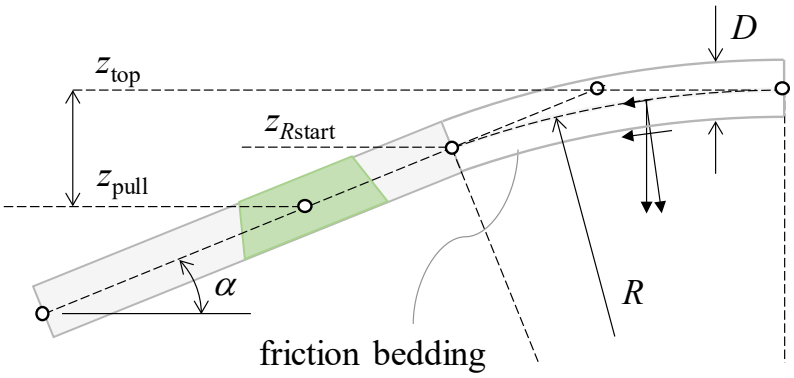

Fig. 5. Model definition including curved transition section.

The curved section starts at $z_{Rstart} = z_{top} - R\,(1 - \cos\alpha)$. The x-coordinate of the end of the curve is $x_{top} = x_{Rstart} + R\,\sin\alpha$, with $x_{Rstart} = x_0 + (z_{Rstart} - z_0)\,\cot\alpha$. The force equilibrium in the curved portion is, when pushed upward and experiencing downward friction, given in Fig. 5. The formulas include a loop since the friction depends on the preponderance, which depends on N, which depends on the friction.

Looking for a straightforward analytic approach to the evaluation of the model, first a low (frictionless) estimate of N is defined: $N_{low} = (z_{top} - z_i)\,q_s$, with $q_s = (\rho_s - \rho)gD$. The resulting distributed force on the underlayer is: $q_{sz'} = q_s \cos\theta - N_{low}/R$, with $q_{sz'}$ and N_{low} functions of x or θ. This force is used to calculate the force F_2 as indicated in Fig. 6. The estimate of N including friction is defined as $N_{high} = N + F_1 + F_2$ (refer Fig. 7), and the values at any location are found by integration starting from x_{top} downward.

When finding L as a function of P, it needs to be realized that the 'foundation pressure' of the revetment in the curve is reduced due to the normal force deflection. So, L is found by dividing P by $q_{sz'}$ at point 2. The bending moment caused by the load is similarly calculated as: $M_E = {}^1/_{16}\,q_{sz'}\,L^2$.

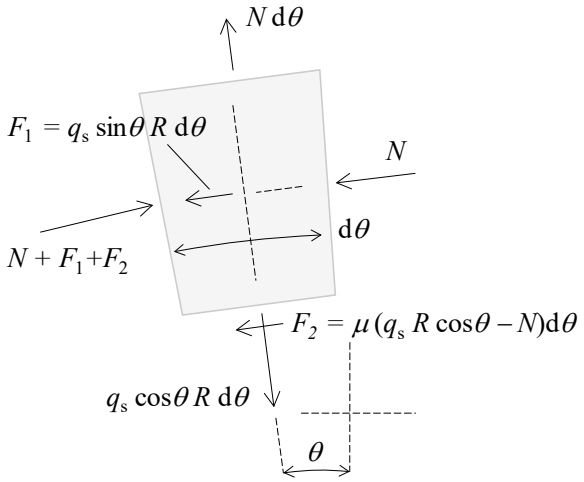

Fig. 6. Definition of forces in curved section

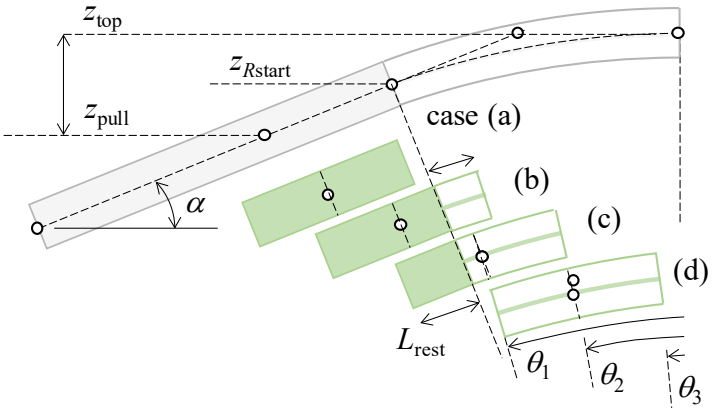

Fig. 7. Definition of cases in curved section

The variables z_{pull} and L determine which of the cases (a) to (d) is applicable (see Fig. 7). Geometric formulas are derived to define the z-values and θ-values of the three points that characterise the confined beam. For the cases (b) and (c), a positive respective negative dimension L_{rest} is defined. For the three points, the normal forces N_{low} and N_{high} can be computed. For the evaluation of the moment resistance, the following values are used:

$$N_1 = N_{high,1}$$
$$N_2 = N_1 + (N_{low2} - N_{low1})$$
$$N_3 = N_2 + (N_{low3} - N_{low2}) \quad (4)$$

The load effect M_E and the resistance M_R are set equal in order to find P at a certain location.

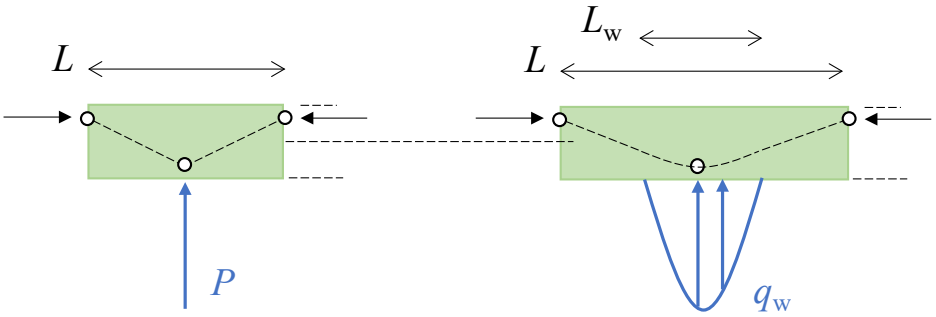

Fig. 8. Analytical beam model with uplift pressure over finite length of the beam.

In reality, the uplift load is not a concentrated force *P,* but a distributed load the acts over a certain length L_w of the beam (see Fig. 8). The equilibrium includes the parameter L_w that is related to the permeability of the revetment. Based on earlier verified theory, the length L_w can be taken as 3 or 4 times the leakage length (for its definition refer to Agema et al. 1986). In this paper, the leakage length was taken as 1.5 *D*, resulting in an uplift length L_w of approximately 0.6m (test scale). The corresponding formulas for the bending moment are given in (Peters, 2017). For the case $L_w < L$:

$$\frac{M_E}{q_s \cdot {L_w}^2} = -0.0289 \cdot \left(\frac{q_w}{q_s}\right) + 0.0253 \left(\frac{q_w}{q_s}\right)^2 \quad (5)$$

The results of the analytical model are presented in Fig. 12, showing the vertical coordinate of the point of wave attack on the vertical axis and the available resistance in the various models on the horizontal axis. The results show that wedged interlocking elements provide additional stability compared to the straight model. Furthermore, the model with the curved top part provides additional stability on top of that.

3 Experiment set-up and tests

Scale model tests were conducted in the Large Wave Flume (GWK) of the Coastal Research Centre (FZK), joint research facility of the Leibniz University Hannover and Technical University Braunschweig. The GWK is 307 m long, 7 m deep and 5 m wide. The model was constructed to a scale of 1:5. The Froude scaling law was applied since gravitational forces, pressures and inertia forces are dominant for the model.

The torqued concrete columns were tested as a part of a complete dike design, which included a foreshore, a toe protection, a lower slope, a berm and an upper slope with roughness elements. The revetments were constructed on top of a sand core. The foreshore started at 224.11 meters from the wave piston and 41.04 m before the lower end of the revetment slope. The bottom of the flume (form which the waterdepth in table 1 is measured) was 4.03 meter below the lower end of the lower revetment slope. The 0.12 m thick torqued concrete columns were placed on a bed of fine granular

material (8-14 mm). The concrete columns in the upper curve had a density of 2800 kg/m^3, while the other concrete columns had a density of 2400 kg/m^3. Fig. 9 presents a cross-section of the lower slope.

Waves were generated with a piston type wave generator equipped with active wave absorption. The maximum stroke of the wave paddle was approximately ± 2.10 m. In total, 29 wave tests were performed aiming at generating 500 waves. Some tests, however, had to be aborted preliminary due to cross oscillations caused by the high wave steepness that was specified for the project. All wave series were conducted with a JONSWAP spectrum. For this paper, six tests are selected which have waves around the design load and water levels near the top of the revetment. Table 1 presents the details of these tests:

Tab. 1. Overview of analysed tests

Test number	Water depth [meter]	Wave height H_{m0} [meter]	Peak wave period T_p [second]	Test duration [second]
2017120602	5.00	0.82	3.41	1170
2017120604	4.78	0.70	3.20	1670
2017120605	4.78	0.83	3.41	1670
2017120606	4.78	0.90	3.57	1490
2017120703	4.93	0.89	3.44	1670
2017120801	4.78	0.98	3.65	1670

The model tests were instrumented. For this paper, normal force and pressure transducer measurements are presented. Other relevant instrumentation for the torqued concrete columns included wave gauges, ultrasonic distance sensors (to measure wave breaker heights), 3D laser scanner (to measure deformations) and lateral force measurements.

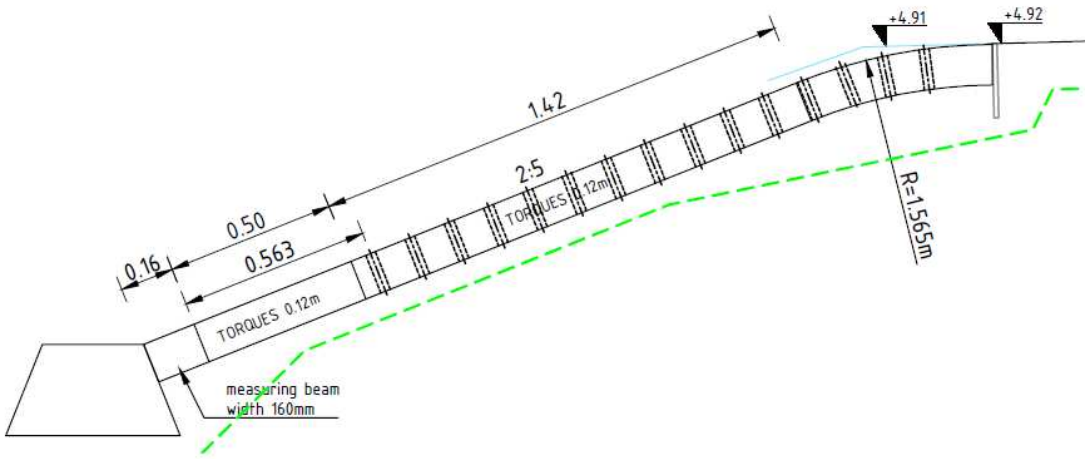

Fig. 9. Model set-up.

4 Results

The normal forces in the revetment, acting on the toe beam were measured by a northern and a southern load cell, each with a capacity of 10 kN. The load cells were placed directly on the toe beam. A stiff steel beam (HEM 100 profile) was then placed over the load cells, while the lower revetment rested directly on the beam. As expected, normal forces in the toe increased to approximately 100% of the weight of the revetment during the complete test program (see Fig. 10).

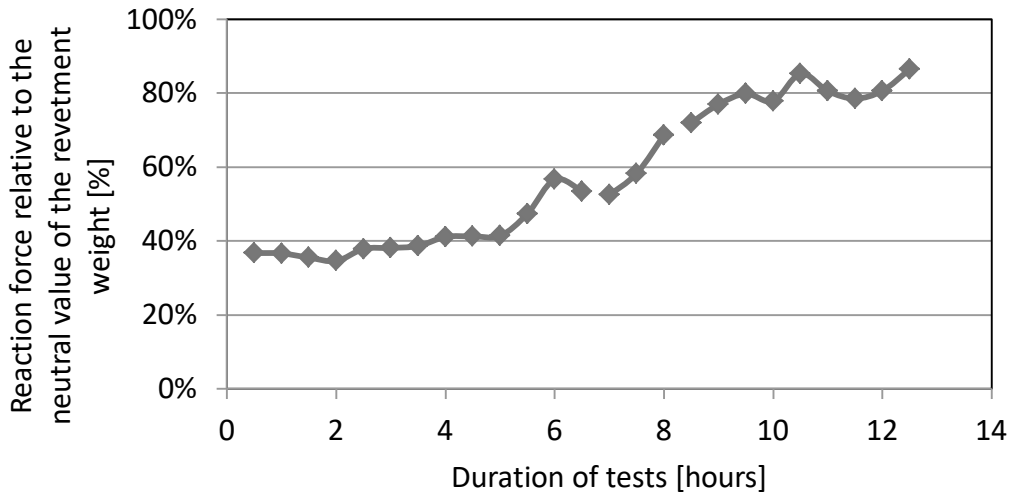

Fig. 10. Normal force measurements.

Pressures were measured at a sampling frequency of 2 kHz above and below the lower revetment. A total of fifteen pressure transducers with a capacity of 5 bar were located at the top of the revetment. These pressure transducers measured the wave impacts on the lower revetment. The wave pressures in the filter layer were measured by pressure transducers with a capacity of 1 bar.

The peak pressures at the top of the revetment were collected per wave. Only the twenty highest peaks were selected for further analysis, as these peaks provide most insight in the design uplift load. For these highest peaks, the neighbouring sensors and the signal -0.1/+0.2 seconds were reviewed to check for measurement errors. On average, fifteen peaks were analysed in more detail to relate the hydraulic loads to the results of other studies. Fig. 11 (left) presents the relative wave impact pressure related to the breaker parameter, while Fig. 11 (right) indicates the net water pressure below the revetment. As can be seen in these figures, the hydraulic loads were, generally, found to be lower than other scale model results.

These relatively low loads are believed to be caused by hydraulic effects introduced by the berm and upper slope. Relatively thick water layers on the revetment were observed during wave impacts. The combination of the rough upper revetment and berm were able to temporarily hold large amounts of water and release it relatively slowly. Consequently, wave run-down occurred and coincided with much thicker water layers (~ 1 m prototype scale) compared to other tests (~ decimetres prototype scale). The wave impacts were dampened by turbulence in these thick water layers, resulting in reduced impact pressures at the level of the top of the revetment.

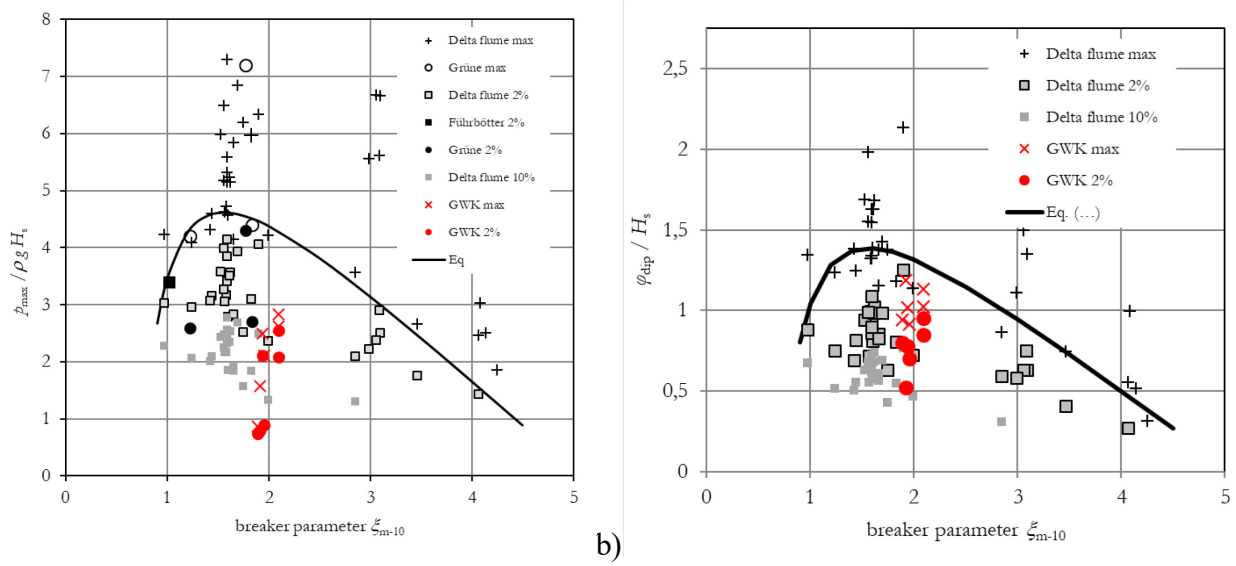

a) b)

Fig. 11. Wave impact p_{max} (left) and hydraulic load on revetment φ_{dip} (right) compared with the breaker parameter (adjusted from Peters, 2017).

The uplift loads can now be compared with the analytical model from the second paragraph. As no significant damage was observed during the tests, the uplift loads were expected to be lower than the resistance found in the model. Sinusoidal shaped loads on the revetment were recorded with a width ranging from 0.3 to 0.6 meter (1.5 to 3 meter prototype scale). Conservatively, a load length of 0.6 meter was applied to determine the moment capacity according to the model. Fig. 13 relates the peak uplift pressures to the location relative to the top of the revetment. Most loads are found to be below the expected resistance. A significant number of wave impact loads exceed the resistance based on a normal straight sliding model. A very limited number of impact loads are slightly above the values obtained by a resistance model based on the curved section with wedge interlocking elements, as some load lengths are shorter than assumed (< 0.6m). Overall, the measured loads seem to confirm the validity of the resistance model and confirm the necessity of applying interlocking elements and a curved top section.

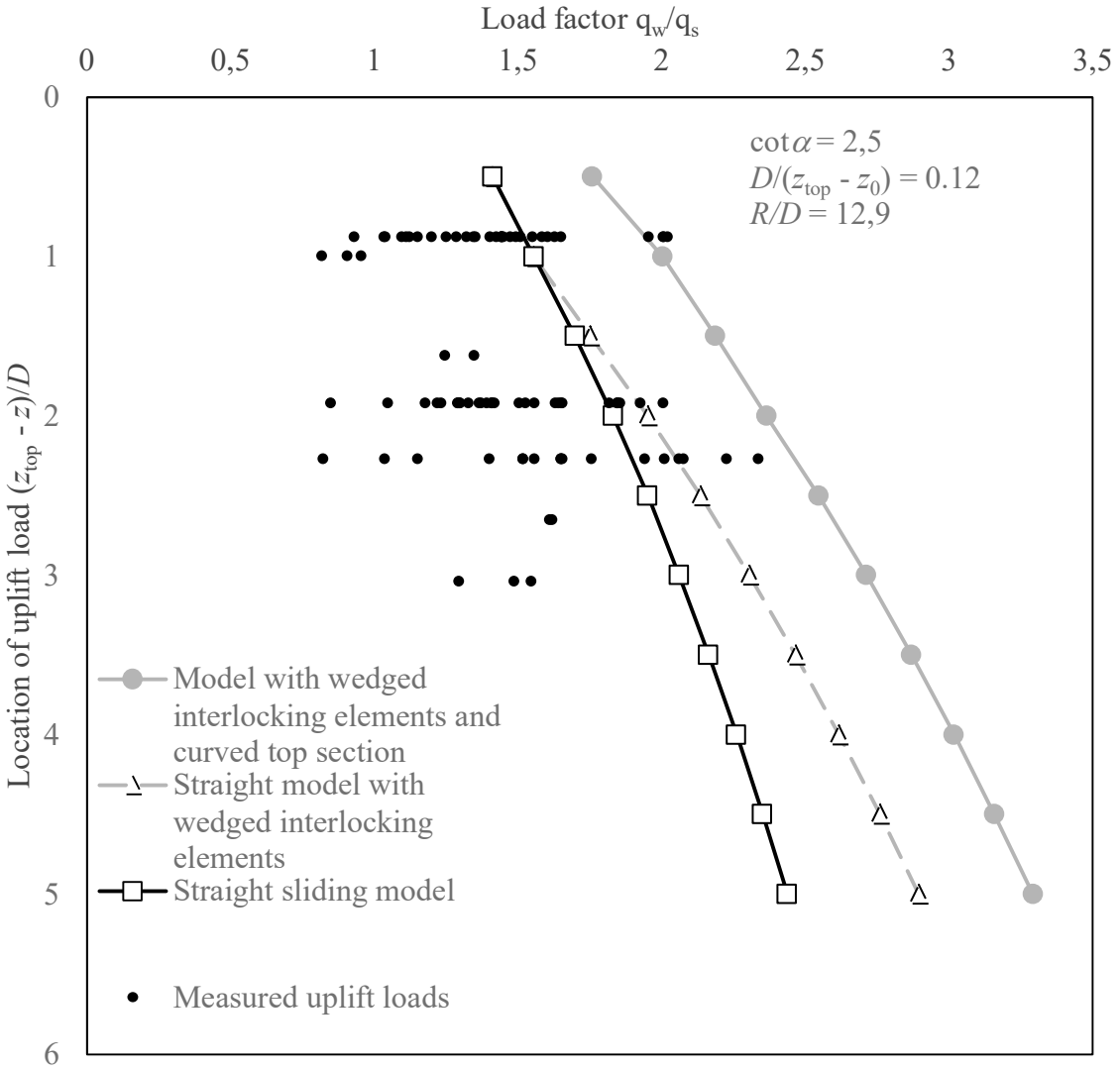

Fig. 12. Measured net uplift pressures compared to the analytical mechanical model.

Discussion

Normal concrete columns are suitable to withstand high hydraulic loads. Generally, it is recommended to extend this revetment type well above the point of attack to generate sufficient axial pre-load of the revetment beam. However, when the top of the revetment is located below the design water level, normal concrete columns cannot resist high hydraulic loads. The large-scale flume experiments confirm the necessity of interlocking columns with a curved top at this section of the revetment. Torqued concrete columns can be placed in a curve and are found to be a suitable solution for the upper part of the revetment.

This paper provides a mechanical model that is able to calculate and value the additional strength provided by interlocking concrete columns and when a curved upper section of the revetment is applied. The analytical mechanical model is able to explain the resistance against many high loads. Large scale model tests confirmed the validity of the model. Therefore, the model is suitable for design purposes. Optionally, 2D-effects spreading local wave load peaks in the cross direction of the flume, and dynamic load effects could be included in the model to better predict mechanical behaviour.

During the large-scale flume tests, no revetment failure occurred. The revetment proved to have at least the same strength as the analytical mechanical model could predict. Additional tests are required to better understand the failure modes of this revetment type.

Acknowledgements

Authors Leslie Mooyaart, Dirk Jan Peters and Menno Huis in ’t Veld were involved in the tender design of the Afsluitdijk in the team of contractor Corneel. Author Nils Kerpen was responsible for the experiment programme. Authors wish to mention Dirk Jan Peters and Rob Torsing (of Zwarts & Jansma Architects) as inventors of the new block type. The authors would like to thank Talia Schoones and Bart Mous for their contribution to the experiments and for reading the manuscript.

References

Agema, J. F., Pilarczyk, K. W., Verheij, H. J., de Quelerij, L., Ebbens, E. H., de Groot, M. B., Stuip, J. et al., 1986. Betonnen bekledingen op dijken en langs kanalen. Edited by J. F. et. al. Agema. VNC.

Bolderman, M. B. N., Dwars, A. W. C., 1919. Waterbouwkunde. 2nd ed. Amsterdam: L. J. Veen.

Huitema T., 1947. Dijken, Kosmos, Antwerpen.

Klein Breteler M. (ed), 1992. Handboek voor dimensionering van gezette taludbekledingen. CUR / TAW report 155.

Peters D. J., 2017. Design of pattern-placed revetments, PhD-thesis, TU Delft.

Schoen S., 2003. Wrijvingsproeven van steenzetting op filter, MSc-thesis, TU Delft.